AIAA 80-0007R

Navier-Stokes Computations of Turbulent Compressible Two-Dimensional Impinging Jet Flowfields

R. K. Agarwal* and W. W. Bower†
McDonnell Douglas Corporation, St. Louis, Mo.

Planar mass-averaged compressible Navier-Stokes and energy equations in stream function/vorticity form are solved in conjunction with a two-equation (k-ϵ) turbulence model for impinging jet configurations relevant to VTOL aircraft design. The physical domain of the flow is mapped conformally into a rectangular computational region. An augmented central-difference scheme is used to preserve the diagonal dominance character of the difference equations at high Reynolds numbers. The resulting difference equations are solved by successive point relaxation. Excellent agreement with the experimental data is obtained for the airframe undersurface pressure, ground-plane pressure, and the centerline velocity decay along the jet axis. Computed turbulent kinetic energy along the jet axis, however, has a larger overshoot near the ground plane than indicated by the experimental data.

Nomenclature

C_p = coefficient of specific heat
D = width of the entering jet in physical plane
Fr = Froude number, $= V_0/\sqrt{gD}$
g = acceleration due to gravity
h = mass-averaged static enthalpy
H = height of the jet above the gound plane
k = mass-averaged turbulent kinetic energy
k_{th} = coefficient of heat conduction
L = turbulence length scale, $= \bar{k}^{3/2}/\bar{\epsilon}$
M = Mach number, $= V_0/\sqrt{\gamma RT_0}$
n = coordinate normal to the boundary
p = mass-averaged static pressure
Pr = Prandtl number, $\mu_0 c_{p_0}/k_{th0}$
Pr_t = turbulent Prandtl number
R = gas constant
Re = Reynolds number, $= \rho_0 V_0 D/\mu_0$
Re_F = Reynolds number, $= \rho_0 V_F D_F/\mu_0$
T = mass-averaged static temperature
u,v = mass-averaged x and y components of velocity, respectively
V_0 = velocity at the centerline of the entering jet in the physical plane
W = width of the computational domain
x = abscissa
y = ordinate
γ = ratio of the specific heats, $= 1.4$
λ,χ = stretching function in the y and x directions, respectively
μ = coefficient of viscosity
μ_t = eddy viscosity coefficient
μ_{eff} = $\mu + \mu_t$
ρ = density
ϵ = mass-averaged turbulent dissipation
ω = mass-averaged vorticity
ψ = mass-averaged stream function
ξ,η = conformally transformed $\bar{x}$ and $\bar{y}$ coordinate in the computational plane, respectively
ϕ = ($\bar{\psi},\bar{\omega},\bar{\rho},\bar{h},\bar{k}$, or $\bar{\epsilon}$)

Subscripts

0 = conditions on the centerline of the entering jet
F = conditions at the boundary of the computational domain
w = conditions at the wall

Superscript

$\bar{()}$ = nondimensional quantity

Introduction

An important consideration in vertical takeoff and landing (VTOL) aircraft design is the aerodynamic interaction between airframe undersurfaces and the ground in the presence of the lift jets. Turbulent lifting jets mix with their surroundings leading to an induced downflow of air around the aircraft and a resulting suck-down force. In addition, the lifting jets impinge upon the ground and create wall jets, which collide to form a stagnation region from which a fountain emerges and impinges on the fuselage.

Because of the complex nature of the flowfield characterized by turbulent lift jets, wall jets, a stagnation region, and a recirculating region, its analysis necessarily requires solution of the complete time-averaged Navier-Stokes equations in conjunction with a turbulence model. Although the flowfield about a complete VTOL aircraft cannot be calculated at the present time using the time-averaged Navier-Stokes equations, the isolated region of the flow can be computed with this approach. The information obtained can be applied to optimize VTOL aircraft design.

The majority of flowfield analyses carried out to date for the jet impingement problem have been for an isolated jet in ground effect. The inviscid rotational flow model,[1] which has been used to predict the ground-plane pressures, is inadequate because it cannot be used to predict the pressure forces on the airframe caused by induced secondary flow. Furthermore, it cannot take into account the effect of Reynolds number and, for hot jets, the heating of the ground and the airframe. Other alternative approaches,[2,3] which proceed by dividing the flowfield into separate interacting regions that are later coupled to provide the overall solution, have achieved only limited success. Recently, attempts have been made to obtain the numerical solution of the time-averaged Navier-Stokes equations in conjunction with a single-equation turbulence model.[4-6] These studies, however, require the specification of turbulence length scales in the entire computational domain. Wolfshtein[4] specified a constant length scale over the entire flowfield except near the solid boundary, while Kotansky and

Presented as Paper 80-0007 at the AIAA 18th Aerospace Sciences Meeting, Pasadena, Calif., Jan. 14-16, 1980; submitted Jan. 16, 1980; revision received Aug. 3, 1981.

*Scientist, McDonnell Douglas Research Laboratories. Member AIAA.

†Scientist, McDonnell Douglas Research Laboratories. Associate Fellow AIAA.

Bower[5] arbitrarily specified a scale distribution. It is felt, therefore, that a more advanced analysis of the jet-impingement problem should aim toward solution of the Navier-Stokes equations in conjunction with a two-equation turbulence model. To the authors' knowledge, the present investigation is the first attempt in this direction for jet-impingement flows.

In this paper, numerical solutions of the incompressible and compressible time-averaged Navier-Stokes equations are obtained at high Reynolds number using a two-equation turbulence model. The conservation equations are solved in stream function/vorticity form. A numerical conformal mapping is used to transform the nonrectangular physical plane into a rectangular computational plane. An augmented central-difference scheme, which is second-order accurate and stable for all Reynolds numbers, is applied to the transformed differential equations. The discretized system is solved iteratively using successive point relaxation for a range of dimensionless parameters that characterize the problem. Comparisons with experiments show a definite improvement in predictions using a two-equation turbulence model, in contrast to the results obtained with a single-equation turbulence model. The present study also provides an important test case for various turbulence models because it incorporates a number of features of free shear-layer, wall-jet, stagnation-point, and recirculating flows.

In the following sections, the flowfield model, numerical solution scheme, and representative results are presented.

Analysis of Two-Dimensional Impinging Jets

In this section, the procedure is described for computing the incompressible and compressible turbulent flowfields for the unvectored planar lift jet in ground effect shown in Fig. 1. The jet exits from a slot of width D in a contoured upper surface a distance H above the ground plane. The region of interest extends a distance W on each side of the jet centerline. The flowfield can be characterized by three regions: a free-jet region in which the flow is essentially the same as that of a jet issuing into an unbounded region of the same fluid; the impingement region in which the flow changes direction with a large pressure gradient; and the wall-jet region in which the flow traverses the surface with zero pressure gradient. The fluid surrounding the jet is entrained at its boundaries in all three regions. This entrainment results in an induced secondary flow which can produce suck-down forces on the airframe undersurface.

Governing Equations

The governing equations are the time-averaged continuity, momentum (Navier-Stokes), and thermal energy equations for steady compressible flow. These equations have been derived by Rubesin and Rose[7] in the mass-averaged variable form introduced by Favre.[8] In initial work on the planar jet,[5,6] one-equation models were used to represent the turbulence field (the Wolfshtein model[4] for the incompressible jet and Rubesin's extension of the Glushko model[9] for the compressible jet). Both of these approaches suffer because the turbulence length-scale distributions, which are generally unknown for complex flows, must be specified. For this reason, the present analyses of the incompressible and compressible planar jets have used the two-equation Jones-Launder turbulence model[10] in which the length-scale variations are implicit in the analysis and need not be specified a priori.

In the present approach, the governing equations are written in the stream function/vorticity form. Flow conditions at the centerline of the entering jet are used to nondimensionalize the flow variables, the independent variables, and the property values in the governing equations. In terms of a dimensionless compressible stream function $\bar{\psi}$ defined by

$$\frac{\partial\bar{\psi}}{\partial\bar{y}}=\bar{\rho}\bar{u}, \qquad \frac{\partial\bar{\psi}}{\partial\bar{x}}=-\bar{\rho}\bar{v} \tag{1}$$

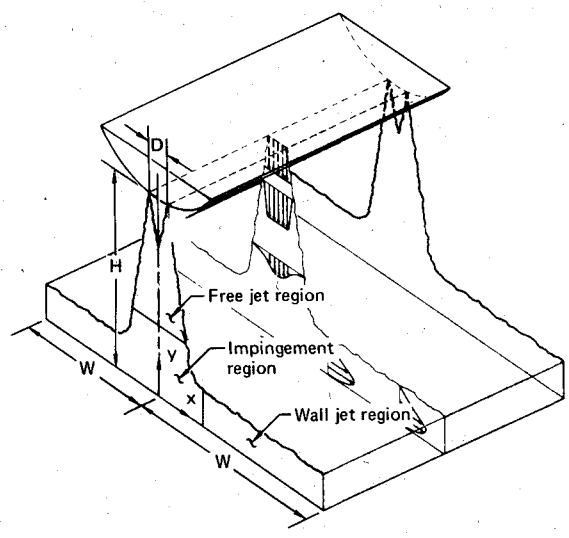

Fig. 1 The planar impinging jet.

and a dimensionless vorticity defined by

$$\bar{\omega}=\frac{\partial\bar{v}}{\partial\bar{x}}-\frac{\partial\bar{u}}{\partial\bar{y}} \tag{2}$$

the dimensionless governing equations are as follows.

Poisson equation for stream function:

$$\frac{\partial^2\bar{\psi}}{\partial\bar{x}^2}-\frac{1}{\bar{\rho}}\frac{\partial\bar{\rho}}{\partial\bar{x}}\frac{\partial\bar{\psi}}{\partial\bar{x}}+\frac{\partial^2\bar{\psi}}{\partial\bar{y}^2}-\frac{1}{\bar{\rho}}\frac{\partial\bar{\rho}}{\partial\bar{y}}\frac{\partial\bar{\psi}}{\partial\bar{y}}=-\bar{\rho}\bar{\omega} \tag{3}$$

Transport equation for vorticity:

$$\bar{\mu}_{\text{eff}}\left(\frac{\partial^2\bar{\omega}}{\partial\bar{x}^2}+\frac{\partial^2\bar{\omega}}{\partial\bar{y}^2}\right)+\left(2\frac{\partial\bar{\mu}_{\text{eff}}}{\partial\bar{x}}-Re\frac{\partial\bar{\psi}}{\partial\bar{y}}\right)\frac{\partial\bar{\omega}}{\partial\bar{x}}$$
$$+\left(2\frac{\partial\bar{\mu}_{\text{eff}}}{\partial\bar{y}}+Re\frac{\partial\bar{\psi}}{\partial\bar{x}}\right)\frac{\partial\bar{\omega}}{\partial\bar{y}}=Re\phi_1-\phi_2-\frac{Re}{Fr^2}\frac{\partial\bar{\rho}}{\partial\bar{x}} \tag{4}$$

where ϕ_i, $i=1, 2,\ldots, 13$ are given in Ref. 11.

Poisson equation for static pressure:

$$\frac{\partial^2\bar{p}}{\partial\bar{x}^2}+\frac{\partial^2\bar{p}}{\partial\bar{y}^2}=\frac{2}{Re}\left(\frac{\partial^2\bar{\mu}_{\text{eff}}}{\partial\bar{x}^2}\phi_3+\frac{\partial\bar{\mu}_{\text{eff}}}{\partial\bar{x}}\phi_4\right.$$
$$\left.+2\frac{\partial^2\bar{\mu}_{\text{eff}}}{\partial\bar{x}\partial\bar{y}}\phi_5+\frac{\partial\bar{\mu}_{\text{eff}}}{\partial\bar{y}}\phi_6+\frac{\partial^2\bar{\mu}_{\text{eff}}}{\partial\bar{y}^2}\phi_7+\frac{4}{3}\bar{\mu}_{\text{eff}}\phi_8\right)$$
$$-2\phi_9+\frac{2}{Fr^2}\frac{\partial\bar{\rho}}{\partial\bar{y}}-\frac{4}{3}\bar{\rho}\left(\frac{\partial^2\bar{k}}{\partial\bar{x}^2}+\frac{\partial^2\bar{k}}{\partial\bar{y}^2}\right)-\frac{4}{3}\bar{k}\left(\frac{\partial^2\bar{\rho}}{\partial\bar{x}^2}+\frac{\partial^2\bar{\rho}}{\partial\bar{y}^2}\right) \tag{5}$$

The boundary conditions on the pressure are determined through the presure gradients imposed by the component momentum equations,

$$\frac{\partial\bar{p}}{\partial\bar{x}}=\frac{2}{Re}\left(\frac{\partial\bar{\mu}_{\text{eff}}}{\partial\bar{x}}\phi_3+\frac{\partial\bar{\mu}_{\text{eff}}}{\partial\bar{y}}\phi_5+\frac{1}{2}\bar{\mu}_{\text{eff}}\phi_4\right)-2\phi_{10}$$
$$-\frac{4}{3}\left(\bar{\rho}\frac{\partial\bar{k}}{\partial\bar{x}}+\bar{k}\frac{\partial\bar{\rho}}{\partial\bar{x}}\right) \tag{6}$$

$$\frac{\partial \bar{p}}{\partial \bar{y}} = \frac{2}{Re}\left(\frac{\partial \bar{\mu}_{\text{eff}}}{\partial \bar{x}}\phi_5 + \frac{\partial \bar{\mu}_{\text{eff}}}{\partial \bar{y}}\phi_7 + \frac{1}{2}\bar{\mu}_{\text{eff}}\phi_6\right) - 2\phi_{11} + \frac{2}{Fr^2}\bar{\rho} - \frac{4}{3}\left(\bar{\rho}\frac{\partial \bar{k}}{\partial \bar{y}} + \bar{k}\frac{\partial \bar{\rho}}{\partial \bar{y}}\right) \tag{7}$$

Transport equation for thermal energy:

$$\frac{1}{Pr}\frac{\bar{k}_{\text{eff}}}{\bar{c}_p}\left(\frac{\partial^2 \bar{h}}{\partial \bar{x}^2} + \frac{\partial^2 \bar{h}}{\partial \bar{y}^2}\right) + \left[\frac{1}{Pr}\frac{\partial}{\partial \bar{x}}\left(\frac{\bar{k}_{\text{eff}}}{\bar{c}_p}\right) - Re\frac{\partial \bar{\psi}}{\partial \bar{y}}\right]\frac{\partial \bar{h}}{\partial \bar{x}} + \left[\frac{1}{Pr}\frac{\partial}{\partial \bar{y}}\left(\frac{\bar{k}_{\text{eff}}}{\bar{c}_p}\right) + Re\frac{\partial \bar{\psi}}{\partial \bar{x}}\right]\frac{\partial \bar{h}}{\partial \bar{y}} = \frac{Re}{2\bar{\rho}}\left(\frac{\partial \bar{\psi}}{\partial \bar{x}}\frac{\partial \bar{p}}{\partial \bar{y}} - \frac{\partial \bar{\psi}}{\partial \bar{y}}\frac{\partial \bar{p}}{\partial \bar{x}}\right) - \phi_{12} - \frac{Re}{Fr^2}\frac{\partial \bar{\psi}}{\partial \bar{x}} - \frac{2}{3}\frac{Re\bar{k}}{\bar{\rho}}\left(\frac{\partial \bar{\rho}}{\partial \bar{y}}\frac{\partial \bar{\psi}}{\partial \bar{x}} - \frac{\partial \bar{\rho}}{\partial \bar{x}}\frac{\partial \bar{\psi}}{\partial \bar{y}}\right) \tag{8}$$

Transport equation for turbulent kinetic energy:

$$\bar{\mu}_k\left(\frac{\partial^2 \bar{k}}{\partial \bar{x}^2} + \frac{\partial^2 \bar{k}}{\partial \bar{y}^2}\right) + \left(\frac{\partial \bar{\mu}_k}{\partial \bar{x}} - Re\frac{\partial \bar{\psi}}{\partial \bar{y}}\right)\frac{\partial \bar{k}}{\partial \bar{x}} + \left(\frac{\partial \bar{\mu}_k}{\partial \bar{y}} + Re\frac{\partial \bar{\psi}}{\partial \bar{x}}\right)\frac{\partial \bar{k}}{\partial \bar{y}} = Re\left[-\frac{\phi_{13}}{Re} + \frac{2}{3}\frac{\bar{k}}{\bar{\rho}}\left(\frac{\partial \bar{\rho}}{\partial \bar{y}}\frac{\partial \bar{\psi}}{\partial \bar{x}} - \frac{\partial \bar{\rho}}{\partial \bar{x}}\frac{\partial \bar{\psi}}{\partial \bar{y}}\right) + \bar{\rho}\bar{\epsilon} + \frac{2\bar{\mu}}{Re}\left(\frac{\partial \sqrt{\bar{k}}}{\partial \bar{y}}\right)^2\right] \tag{9}$$

Transport equation for turbulent dissipation

$$\bar{\mu}_\epsilon\left(\frac{\partial^2 \bar{\epsilon}}{\partial \bar{x}^2} + \frac{\partial^2 \bar{\epsilon}}{\partial \bar{y}^2}\right) + \left(\frac{\partial \bar{\mu}_\epsilon}{\partial \bar{x}} - Re\frac{\partial \bar{\psi}}{\partial \bar{y}}\right)\frac{\partial \bar{\epsilon}}{\partial \bar{x}} + \left(\frac{\partial \bar{\mu}_\epsilon}{\partial \bar{y}} + Re\frac{\partial \bar{\psi}}{\partial \bar{x}}\right)\frac{\partial \bar{\epsilon}}{\partial \bar{y}} = Re\left[-\frac{C_1\bar{\epsilon}}{\bar{k}}\frac{\phi_{13}}{Re} + \frac{2}{3}\frac{C_1\bar{\epsilon}}{\bar{\rho}}\left(\frac{\partial \bar{\psi}}{\partial \bar{x}}\frac{\partial \bar{\rho}}{\partial \bar{y}} - \frac{\partial \bar{\rho}}{\partial \bar{x}}\frac{\partial \bar{\psi}}{\partial \bar{y}}\right) - \frac{2\bar{\mu}\bar{\mu}_t}{\bar{\rho}^3 Re^2}\left\{\frac{\partial^3 \bar{\psi}}{\partial \bar{y}^3} - \frac{2}{\bar{\rho}}\frac{\partial \bar{\rho}}{\partial \bar{y}}\frac{\partial^2 \bar{\psi}}{\partial \bar{y}^2} + \frac{2}{\bar{\rho}^2}\frac{\partial \bar{\psi}}{\partial \bar{y}}\left(\frac{\partial \bar{\rho}}{\partial \bar{y}}\right)^2 - \frac{1}{\bar{\rho}}\frac{\partial \bar{\psi}}{\partial \bar{y}}\frac{\partial^2 \bar{\rho}}{\partial \bar{y}^2}\right\}^2 + \frac{C_2 f_2 \bar{\rho}\bar{\epsilon}^2}{\bar{k}}\right] \tag{10}$$

Jones-Launder turbulence-model relations:

$$f_2 = 1 - 0.3\exp(R_t^2), \quad \bar{\mu}_t = \bar{\mu}c_\mu f_\mu R_t$$

$$f_\mu = \exp\left[\frac{-2.5}{1 + R_t/50}\right], \quad \bar{\mu}_k = \bar{\mu} + \lambda_k\bar{\mu}_t$$

$$\bar{\mu}_\epsilon = \bar{\mu} + \lambda_\epsilon\bar{\mu}_t, \quad \bar{\mu}_{\text{eff}} = \bar{\mu} + \bar{\mu}_t$$

$$\frac{\bar{k}_{\text{eff}}}{\bar{c}_p} = \frac{\bar{k}_{th}}{\bar{c}_p} + \bar{\mu}_t\frac{Pr}{Pr_t}, \quad R_t = \frac{\bar{\rho}\bar{k}^2}{\bar{\mu}\bar{\epsilon}}$$

$$\lambda_k = 1, \quad \lambda_\epsilon = 0.9091, \quad Pr_t = 0.9$$

$$C_1 = 1.44, \quad C_2 = 1.92, \quad c_\mu = 0.09 \tag{11}$$

The system of equations is completed with the equations of state,

$$\bar{p} = 2\bar{\rho}\left(\frac{\gamma - 1}{\gamma}\right)\bar{h} \tag{12}$$

$$\bar{h} = \bar{c}_p\bar{T} \tag{13}$$

The temperature variation of the transport properties is given by Worsøe-Schmidt and Leppert,[12]

$$\bar{\mu} = (\bar{h}/\bar{h}_0)^{0.67} \tag{14}$$

$$\bar{k}_{th} = (\bar{h}/\bar{h}_0)^{0.71} \tag{15}$$

For the case of incompressible flow ($\bar{\rho} = 1$), the previous equations are greatly simplified both in form and number. Equations (8) and (12-15) are not needed; also the Poisson equation for static pressure need not be solved simultaneously with the Poisson equation for stream function and the vorticity transport equation.

Numerical Solution Scheme

To solve the flowfield equations for a planar jet discharging from a curved surface, as shown in Fig. 1, a conformal mapping technique is used to map the irregular physical plane into a rectangular computational plane. The governing equations are then rewritten in terms of the computational plane coordinates. Since there is geometric symmetry with respect to the jet centerline, only half of the flowfield is treated.

The mapping technique, which is an inverse procedure, was devised at MDRL by Hoffman[13] and is best explained with reference to Fig. 2. Initially, a finite-difference computational plane with coordinates (ξ,η) is specified. Stretching functions are then applied in each coordinate direction

$$\chi = f_1(\xi) \tag{16}$$

and

$$\lambda = f_2(\eta) \tag{17}$$

With these relations, a mapping plane (χ,λ) is determined which permits finer resolution of the flowfield in regions where the gradients of the computed variables are severe. Finally, a conformal mapping given by

$$\chi + i\lambda = F(\bar{x} + i\bar{y}) \tag{18}$$

is introduced which specifies the physical plane $(\bar{x},\bar{y})$. Since the mapping [Eq. (18)] holds, it follows that both $\bar{x}$ and $\bar{y}$ obey Laplace equations with coordinate stretching

$$\frac{d\xi}{d\chi}\frac{\partial}{\partial \xi}\left(\frac{d\xi}{d\chi}\frac{\partial \bar{y}}{\partial \xi}\right) + \frac{d\eta}{d\lambda}\frac{\partial}{\partial \eta}\left(\frac{d\eta}{d\lambda}\frac{\partial \bar{y}}{\partial \eta}\right) = 0 \tag{19}$$

$$\frac{d\xi}{d\chi}\frac{\partial}{\partial \xi}\left(\frac{d\xi}{d\chi}\frac{\partial \bar{x}}{\partial \xi}\right) + \frac{d\eta}{d\lambda}\frac{\partial}{\partial \eta}\left(\frac{d\eta}{d\lambda}\frac{\partial \bar{x}}{\partial \eta}\right) = 0 \tag{20}$$

The boundary conditions imposed on Eqs. (19) and (20) follow from physical constraints when they are known at the boundaries and from integration of the Cauchy-Riemann relations,

$$\frac{d\xi}{d\chi}\frac{\partial \bar{x}}{\partial \xi} = \frac{d\eta}{d\lambda}\frac{\partial \bar{y}}{\partial \eta} \tag{21}$$

and

$$\frac{d\eta}{d\lambda}\frac{\partial \bar{x}}{\partial \eta} = -\frac{d\xi}{d\chi}\frac{\partial \bar{y}}{\partial \xi} \tag{22}$$

when the $\bar{x}$ and $\bar{y}$ boundary distributions are not known.

In the present mapping scheme, instead of specifying the coordinate distributions in the physical plane and accepting whatever computational plane results, a numerically convenient computational plane is specified, and the corresponding coordinate distributions within the specified physical boundaries are computed.

The mapping equations are discretized using conventional central differences and are solved by a Gauss-Seidel relaxation algorithm.

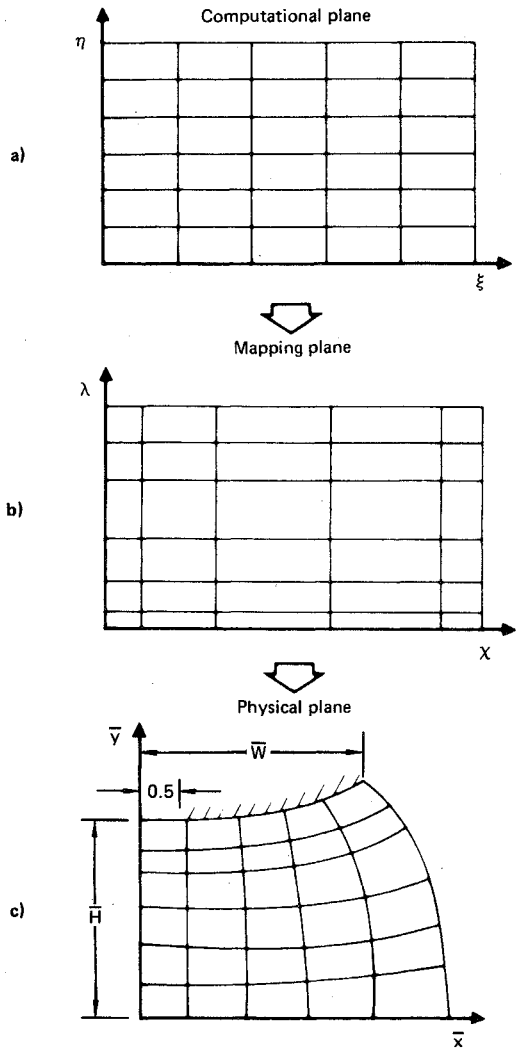

Upper boundary is defined by:

$\bar{y} = \bar{H}, \; 0 \leq \bar{x} \leq 0.5$

$= \bar{H} + 0.003375 - 0.01225\,\bar{x} + 0.00852\,\bar{x}^2 + 0.00496\,\bar{x}^3, \; 0.5 \leq \bar{x} \leq 2.785$

$= \bar{H} + 2.349 - [4.977361 - (\bar{x} - 2.4515)^2]^{1/2}, \; 2.785 \leq \bar{x} \leq 4.6825$

Fig. 2 Inverse conformal mapping with stretching.

The transport equations, Eqs. (3), (4), and (8-10), are discretized using Hoffman's second-order accurate augmented central-difference scheme.[13] This scheme preserves the diagonal dominance character of the difference equations at high Reynolds numbers. The resulting difference equations are solved in sequence by a point successive over relaxation (SOR) algorithm. For each flow variable ϕ, a local residual is defined by $r_\phi = |\phi_{N+1} - \phi_N|$, where N is the iteration counter. Convergence is said to be achieved when $r_\phi < 10^{-6}$ everywhere in the flowfield.

Computed Flowfields

Both the incompressible and compressible flowfields have been calculated for the planar jet of Fig. 1 with and without an upper surface. The physical domain has a height $\bar{H}$ and a width $\bar{W}$. For the general case of compressible flow, the following boundary conditions are imposed: the vorticity, stream function, enthalpy, turbulent kinetic energy, and turbulent dissipation profiles are specified within the entering jet. On the upper computational boundary, in the presence of a solid surface, conditions result from the constraint of a no-slip, impermeable, isothermal wall (in the absence of an upper solid surface, the vorticity, stream function, enthalpy, turbulent kinetic energy, and turbulent dissipation profiles are specified over the entire upper boundary); on the lower surface, conditions result from the constraint of a no-slip, impermeable, adiabatic wall. On the jet centerline the symmetry conditions are imposed, and at the right boundary the flow properties are taken to be uniform with respect to ξ, the transformed $\bar{x}$ coordinate. Pressure gradients at the boundaries are specified using Eqs. (6) and (7). On the no-slip, impermeable wall, boundary vorticity is computed from the relation

$$\bar{\rho}\bar{\omega}_w = -\frac{\partial^2 \bar{\psi}}{\partial \bar{n}^2} \tag{23}$$

where $\bar{n}$ is normal to the boundary into the flow domain.

Computations have been carried out for the following cases.

Case A: Normal impingement of an incompressible turbulent jet on the ground plane (no upper surface). Computations have been carried out for two sets of parameters corresponding to the experimental investigations of Gardon and Akfirat[14] and Schauer and Eustis.[15] In Gardon and Akfirat's experiment, $\bar{H} = 8$ with an exit Reynolds number of 1.1×10^4. In Schauer and Eustis's experiment, $\bar{H} = 40$ with a jet exit Reynolds number of 4.3×10^4. In the computations, a smaller domain with $\bar{H}_F = 1$ and $\bar{W} = 2.5$ was chosen with a grid of 51 nodes in the $\bar{x}$ direction and 41 in the $\bar{y}$ direction. For the computational domain, jet entry conditions were determined using the relations recommended by Schauer and Eustis. These relations can be written as

$$\frac{V_0}{V_F} = \frac{2.35}{\sqrt{(H - H_F)/D_F}} \tag{24}$$

and

$$D/(H - H_F) = 0.22 \tag{25}$$

The Reynolds numbers used in the computations, Re_F, are thus determined to be 1.46×10^4 and 1.27×10^5 for the Gardon-Akfirat and Schauer-Eustis conditions, respectively. On the upper boundary of the computational domain, the following profiles are specified for $\bar{\psi}$, $\bar{\omega}$, $\bar{k}$, and $\bar{\epsilon}$:

$$\bar{\psi} = \tanh(6\xi)/6 \tag{26a}$$

$$\bar{\omega} = 72\bar{\psi}(1 - 36\bar{\psi}^2) \tag{26b}$$

$$\bar{k} = 0.04 \quad \xi \leq \xi \leq 0.4$$

$$= 0.02[1 + \sin\{3\pi/2 - 5\pi(1 - 2\xi)\}] \quad 0.4 \leq \xi \leq 0.5$$

$$= 0 \quad \xi \geq 0.5 \tag{26c}$$

$$\bar{\epsilon} = 5\bar{k}^{3/2} \tag{26d}$$

Figure 3 shows the excellent comparisons of computed ground-plane static pressures with the experimental data. Figure 4 shows the contour plots of the computed flow properties for the Schauer and Eustis case. The stream function plot illustrates the turning of the jet and the mass entrainment. The vorticity distibution shows the convection of $\bar{\omega}$ to the right and the development of the boundary layer on the lower wall. The distributions of the turbulent kinetic energy and the turbulent dissipation illustrate the decay in $\bar{k}$ and $\bar{\epsilon}$ with distance from the jet exit plane except near the ground plane where the turbulent kinetic energy increases rapidly and then quickly drops to zero at the surface.

Case B: Normal impingement of the incompressible turbulent jet on the ground plane in the presence of an upper surface. The computational domain considered is shown in

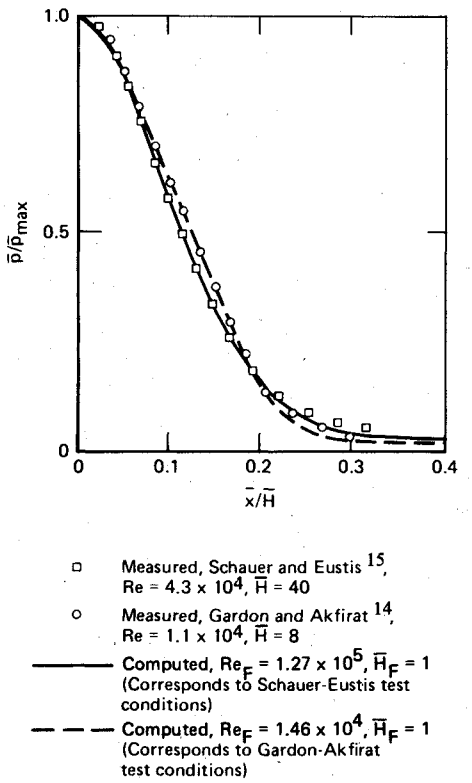

Fig. 3 Comparison of experimental and theoretical ground-plane pressure distributions for the normal impingement of the free upper-boundary planar jet with a fully developed profile.

Fig. 2c with $\bar{H}=2$ and $\bar{W}=3.68$. Computations have been carried out on a 81×41 finite-difference grid for a range of Reynolds numbers from 100 to 130,000. On the upper boundary, in the exit region of the jet, the following profiles are specified for $\bar{\psi}$, $\bar{\omega}$, $\bar{k}$, and $\bar{\epsilon}$:

$$\bar{\psi}=\xi, \quad \xi\le 0.15$$

$$=(1.35-400\xi^3+180\xi^2+120\xi)/147, \quad 0.15\le\xi\le 0.5$$

$$=0.38333, \quad \xi\ge 0.5 \tag{27a}$$

$$\bar{\omega}=0, \quad \xi\le 0.15$$

$$=40(20\xi-3)/49, \quad 0.15\le\xi\le 0.5 \tag{27b}$$

$$\bar{k}=0.04, \quad \xi\le 0.15$$

$$=0.02[1+\sin\{3\pi/2-5\pi(1-2\xi)\}], \quad 0.15\le\xi\le 0.5$$

$$=0, \quad \xi\ge 0.5 \tag{27c}$$

$$\bar{\epsilon}=5\bar{k}^{3/2} \tag{27d}$$

On solid surfaces both $\bar{k}$ and $\bar{\epsilon}$ are taken to be zero.

A comparison of the computed and measured pressure variations of the ground plane and simulated fuselage undersurface is shown in Fig. 5. The agreement is quite good. Figure 6 shows the comparison between the measured and computed centerline variations of the turbulent kinetic energy and velocity. The agreement for the jet centerline velocity decay is excellent; however, the computed turbulent kinetic energy along the jet axis has a larger overshoot near the ground plane than measured in the experiment. This difference can be attributed to a deficiency in the turbulence model, and fine tuning of the various constants used in the model may be required. Nonetheless, the model appears to satisfactorily predict the pressure distribution and the velocity

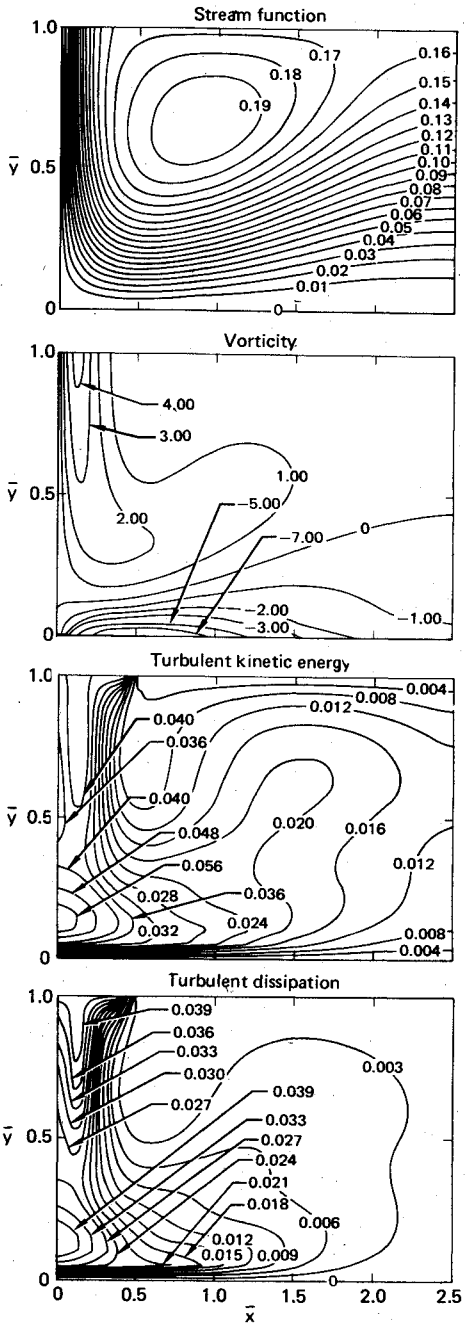

Fig. 4 Property contours for the incompressible free upper-boundary planar jet in ground effect, $\bar{H}_F=1$, $\bar{W}=2.5$, $Re_F=1.27\times10^5$.

field—the quantities of primary interest in VTOL design. Furthermore, as shown in Fig. 5, the two-equation turbulence model used in the present study is superior in prediction than the one-equation turbulence model used in the study of Kotansky and Bower.[5] Based on the results of the present work, it is clear that the intuitive specification of the length scales in previous studies based on a single-equation (k) turbulence model was erroneous, resulting in a large discrepancy between the measurements and prediction. For the present class of flows where there is no single dominant flow direction and there is a large recirculating region, the necessity of a two- or higher-equation turbulence model is established clearly. The turbulence length scale is Reynolds number dependent, as shown in Fig. 7 where the length scale contours are sketched for Reynolds numbers of 100, 10,000, and 130,000. The significant difference in length scales is noticeable in the recirculating region. At higher Reynolds

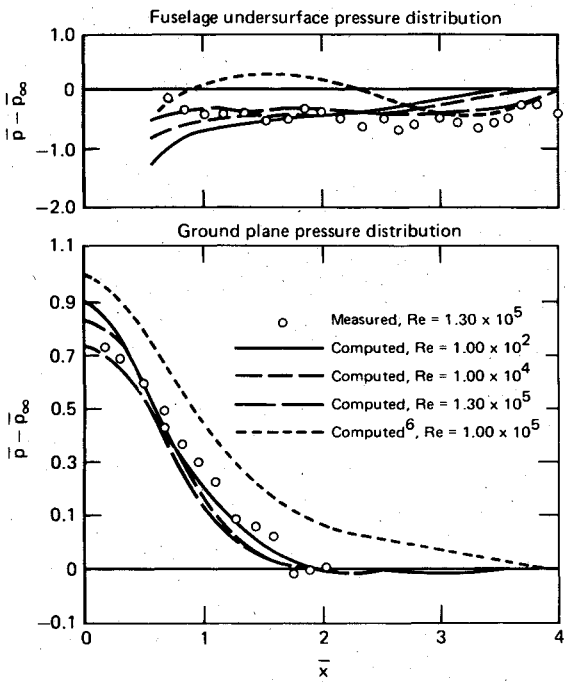

Fig. 5 Comparison of experimental and theoretical pressure distributions for the incompressible planar jet in-ground effect, $\bar{H}=2$, $\bar{W}=3.68$.

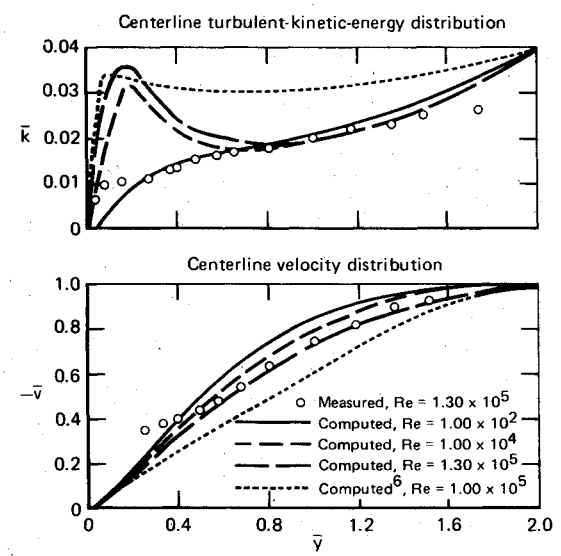

Fig. 6 Comparison of experimental and theoretical centerline property distributions for the incompressible planar jet in-ground effect, $\bar{H}=2$, $\bar{W}=3.68$.

number, the recirculating turbulent zone has larger scales than at low Reynolds numbers.

Figure 8 shows the contour plots of the computed dimensionless variables for high Reynolds number ($Re=130{,}000$) impingement. Again, the stream function plot illustrates the turning of the jet and the mass entrainment. The vorticity distribution shows the convection of $\bar{\omega}$ to the right and the development of boundary layers on the upper wall (where separation occurs at the point of $\bar{\omega}=0$) and on the lower wall. The static pressure plot shows an increase in $\bar{p}$ going toward the stagnation point. Contours of $\bar{k}$ show the regions of decay and increase in the levels of turbulent kinetic energy.

Case C: Normal impingement of the compressible jet on the ground plane in the presence of an upper surface. The computational domain considered is shown in Fig. 2c with

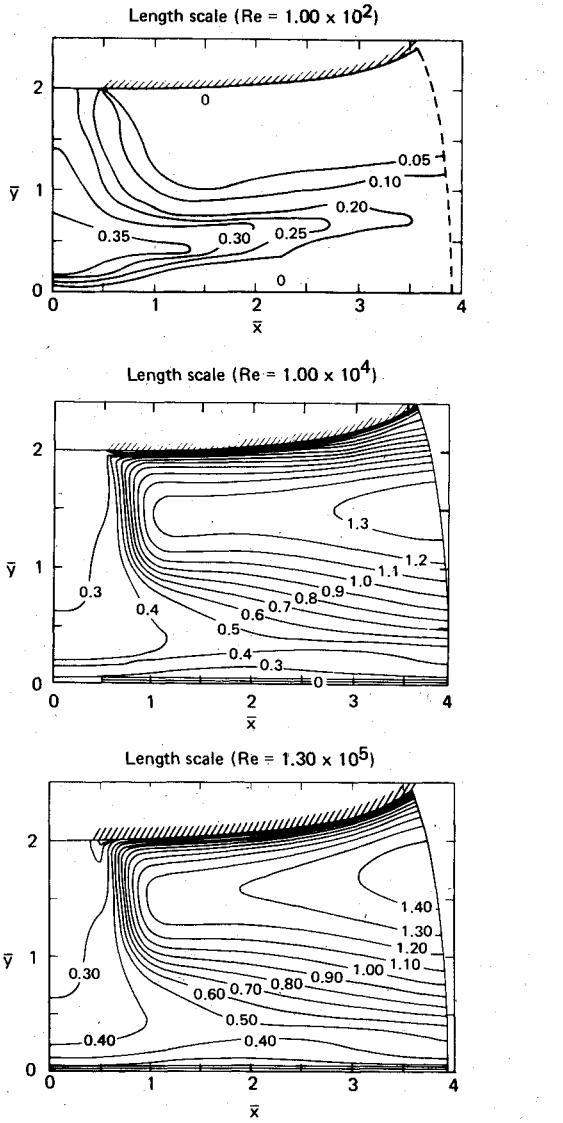

Fig. 7 Turbulent length scale contours at different Reynolds numbers for the incompressible planar jet in-ground effect, $\bar{H}=2$, $\bar{W}=3.68$.

$\bar{H}=2$ and $\bar{W}=3.68$. Computations have been carried out on an 81×41 finite-difference grid for the following set of parameters:

$$M=0.275,\quad Pr=0.68,\quad Re=1.58\times10^5,\quad Fr=1.79\times10^2$$

$$\bar{h}_w=24.728,\quad \bar{h}_0=33.061$$

This set of parameters corresponds to the actual test conditions in the experiment conducted at McDonnell Douglas Research Laboratories. In the computations, in the exit region of the jet, the profiles for $\bar{\psi}$, $\bar{\omega}$, $\bar{k}$, and $\bar{\epsilon}$ are the same as in case B given by Eqs. (27a-d). In addition, the static enthalpy profile is specified as

$$\bar{h}=(\bar{h}_0-\bar{h}_w)\{1-(2\xi)^{1.5}\}^2+\bar{h}_w,\quad 0\le\xi\le0.5$$

$$=\bar{h}_w,\quad \xi\ge0.5 \text{ on the upper isothermal surface} \tag{28a}$$

$$\frac{\partial\bar{h}}{\partial\eta}=0 \quad \text{on the lower adiabatic surface} \tag{28b}$$

Figure 9 shows the comparison between the computed and the measured pressure distributions on the ground plane and the

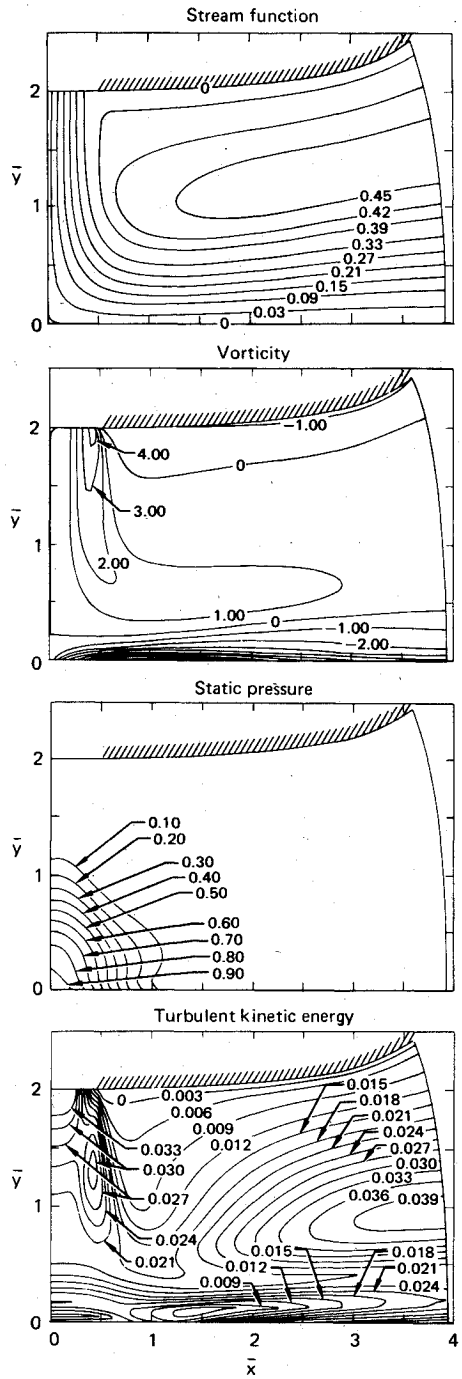

Fig. 8 Property contours for the incompressible planar jet in-ground effect, $\bar{H}=2$, $\bar{W}=3.68$, $Re=1.30\times10^5$.

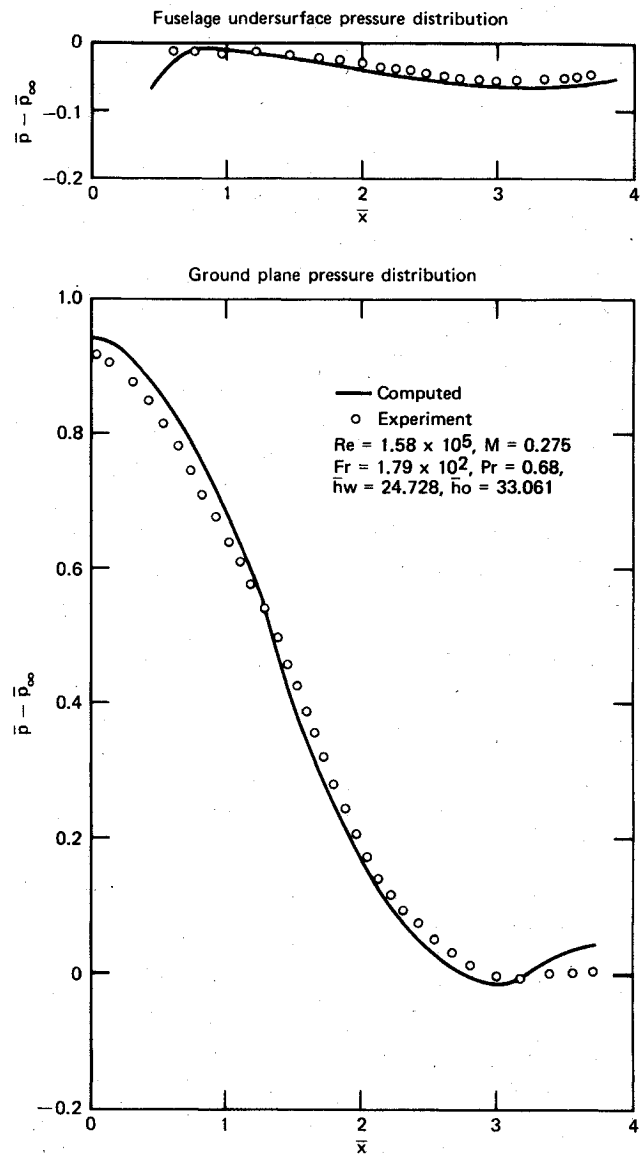

Fig. 9 Comparison of experimental and theoretical pressure distributions for the compressible planar jet in-ground effect, $\bar{H}=2$, $W=3.68$.

airframe undersurface. Once again, the agreement is good. The pressure gradient $\partial\bar{p}/\partial\bar{x}=0$ at $\bar{x}=0$. In the absence of experimental data for other flow quantities, comparison with the computations cannot be made. The contour plots for various flow properties given in Ref. 11 exhibit the qualitative features similar to the incompressible case (Fig. 8) which is to be expected for low subsonic Mach numbers from Morkovin's hypothesis.

Summary

High Reynolds number numerical solutions of the time-averaged Navier-Stokes equations in conjunction with a two-equation $(k-\epsilon)$ turbulence model have been obtained for VTOL ground effect flowfields. The augmented central-difference scheme employed in the computations has been found to be stable as well as fairly accurate at Reynolds numbers of $0(10^5)$. Computation at higher Reynolds numbers, however, requires finer meshes for obtaining reasonable accuracy, as tested primarily by comparison with experiments at high Reynolds number and against other computations at low laminar flow Reynolds numbers. The computed solutions are in good agreement with the experimental data for ground plane, airframe undersurface, and velocity decay along the jet axis. The accuracy of the results close to the solid surface, however, cannot be ascertained because of the lack of skin-friction and surface-temperature data. Furthermore, based on the vast experience with the $(k-\epsilon)$ model for a variety of other aerodynamic flows, it is unlikely that the pressure, the velocity field, the skin friction, and the heating rate all can be predicted accurately using this model. However, the main achievement of the present investigation lies in clearly demonstrating the superiority of the two-equation model for lift-jet configurations over the simpler models in the hierarchy, namely the zero-equation and one-equation models. The flow configurations considered in the present paper provide a good example for conducting future building-block experiments as well as developing advanced modeling techniques in turbulence research.

Acknowledgments

This work was carried out in part under the McDonnell Douglas Independent Research and Development program and in part under Office of Naval Research Contract N00014-76-C-0494.

References

[1]Rubel, A., "Computations of Jet Impingement on a Flat Surface," AIAA Paper 78-207, 1978.

[2]Siclari, M. J., Migdal, D., and Palcza, J. L., "The Development of Theoretical Models for Jet Induced Effects on V/STOL Aircraft," *Journal of Aircraft*, Vol. 13, Dec. 1976, p. 938-944.

[3]Sparrow, E. M. and Lee, L., "Analysis of Flowfield and Impingement Heat/Mass Transfer Due to a Nonuniform Slot Jet," *Journal of Heat Transfer, ASME*, Vol. 97C, 1975, p. 191.

[4]Wolfshtein, "Convection Processes in Turbulent Impinging Jets," Dept. of Mechanical Engineering, Imperial College of Science and Technology, Rept. SF/R/2, Nov. 1967.

[5]Kotansky, D. R. and Bower, W. W., "A Basic Study of the VTOL Ground Effect Problem for Planar Flow," *Journal of Aircraft*, Vol. 15, April 1978, pp. 214-221.

[6]Bower, W. W., "Compressible Viscous Flowfields and Airframe Forces Induced by Two-Dimensional Lift Jets in Ground Effect," Office of Naval Research Rept. ONR-CR215-246-2, March 1978.

[7]Rubesin, M. W. and Rose, W. C., "The Turbulent Mean-Flow, Reynolds-Stress, and Heat-Flux Equations in Mass-Averaged Dependent Variables," NASA TM X-62, March 1973.

[8]Favre, A., "Equations des Gaz Turbulents Compressible," *Journal de Mecanique*, Vol. 4, 1965, p. 361.

[9]Rubesin, M. W., "A One-Equation Model of Turbulence for Use with the Compressible Navier-Stokes Equations," NASA TM-X-73, April 1976.

[10]Jones, W. P. and Launder, B. E., "The Calculation of Low-Reynolds Number Phenomena with a Two-Equation Model of Turbulence," *International Journal of Heat and Mass Transfer*, Vol. 16, June 1973, pp. 1119-1129.

[11]Agarwal, R. K. and Bower, W. W., "Navier-Stokes Computations of Compressible 2-D Impinging Jet Flowfields Using a Two-Equation Turbulence Model," AIAA Paper 80-0007, 1980.

[12]Worsøe-Schmidt, P. M. and Leppert, G., "Heat Transfer and Friction for Laminar Flow of Gas in a Circular Tube at High Heating Rate," *International Journal of Heat and Mass Transfer*, Vol. 8, Oct. 1965, pp. 1281-1302.

[13]Hoffman, G. H., "Calculation of Separated Flows in Internal Passages," *Proceedings of a Workshop on Prediction Methods for Jet V/STOL Propulsion Aerodynamics*, Vol. 1, 1975, pp. 114-124.

[14]Gardon, R. and Akfirat, J. C., "The Role of Turbulence in Determining the Heat Transfer Characteristics of Impinging Jets," *International Journal of Heat and Mass Transfer*, Vol. 8, Oct. 1965, pp. 1261-1272.

[15]Schauer, J. J. and Eustis, R. H., "The Flow Development and Heat Transfer Characteristics of Plane Turbulent Impinging Jets," Dept. of Mechanical Engineering, Stanford University, TR3, Sept. 1963.